Received: 16 January 2020 | Revised: 28 February 2020 | Accepted: 16 April 2020

DOI: 10.1002/rnc.5030

SPECIAL ISSUE ARTICLE

WILEY

Distributed sliding mode control for leader-follower formation flight of fixed-wing unmanned aerial vehicles subject to velocity constraints

Xiangke Wang[1] | **Yangguang Yu**[1] | **Zhongkui Li**[2]

[1]College of Intelligence Science and Technology, National University of Defense Technology, Changsha, China

[2]State Key Laboratory for Turbulence and Complex Systems, Department of Mechanics and Aerospace Engineering, Peking University, Beijing, China

Correspondence
Xiangke Wang, College of Intelligence Science and Technology, National University of Defense Technology, Changsha 410073, China.
Email: xkwang@nudt.edu.cn

Funding information
National Natural Science Foundation of China, Grant/Award Number: 61973309, 61973006

Summary

This paper considers the leader-follower formation flight of fixed-wing unmanned aerial vehicles (UAVs) subject to velocity constraints. A novel distributed sliding mode control law is proposed for each UAV, whose kinematics is described by a unicycle model with a saturated angular velocity and a bounded linear velocity within an interval. The designed control law of each follower UAV only uses its own information and the information of its leader UAV. Driven by the designed control law, the desired formation is achieved with rigorous proof, while the follower UAVs' constraints of both the linear and angular velocities are satisfied. Moreover, the follower's speed adjustment range is relaxed and not required to be strictly larger than their leaders'. Finally, numerical simulations are presented to verify the results.

KEYWORDS

distributed control, fixed-wing UAV, formation control, velocity constraints

1 | INTRODUCTION

Formation control of multiple autonomous vehicles, including unmanned aerial vehicles (UAVs),[1] unmanned ground vehicles[2] and unmanned underwater vehicles,[3] has received many attentions due to its various potential applications, such as cooperative surveillance and searching, cooperative transport, et al.[4,5] A number of control approaches have been proposed for achieving the formation,[6-8] and in general the conventional approaches include the leader-follower method,[9,10] behavior-based method,[11,12] consensus-based method,[13,14] and so on. Among these methods, the leader-follower approach was intensively studied in recent years due to its relatively simple and clear control architecture.[15-20] In the leader-follower approach, a single or multiple UAVs in the formation are assigned as the leaders and fly along a predefined trajectory while the other UAVs, acting as the followers, are to maintain the desired distances and orientations with respect to the leader.[20]

In the past decades, many theoretical achievements have been obtained on the leader-follower formation control problems. In 2002, Das et al proposed a leader-follower local control law for the cooperative control of a group of nonholonomic mobile robots.[15] Based on the work of Das, the formation problem for multiple nonholonomic mobile robots was further analyzed,[16] in which the robots' control inputs were forced to satisfy some constraints that restrict the set of leader's possible paths and admissible positions of the follower with respect to the leader. Further, in order to tackle the case of multiple leaders, the leader-follower formation problem with multiple leaders was investigated and it was shown that the

controllability of a multiagent system can be uniquely determined by the interconnection graph.[17,21-23] The controllability of the leader-follower formation for the multi-agent systems was also discussed.[24] Following this way, Hu and Feng further considered the effect of noise and presented a distributed tracking control scheme for a leader-follower multi-agent system with measurement noises.[18] Afterwards, the cases of switching interconnection topologies were discussed in this paper via both static and dynamic feedback.[19] As the dynamics considered in most previous works are first-order integrators, the leader-follower problem with agents governed by a second-order dynamics was considered in References 25-27. The measurement delays in leader-follower formation control were considered in Chen's work,[28] in which a low-level controller for leader-follower formations of nonholonomic vehicles was designed and the stability of the closed-loop system was proved.

Formation flight of multiple fixed-wing UAVs has attracted significant attentions due to its increasing demands in civil and military domains. However, as a special type of robots, fixed-wing UAVs have some special properties owing to its special dynamics. Firstly, the dynamics of the fixed-wing UAV is an under-actuated system and its kinematics can be simplified into a unicycle system.[29] In addition, the fixed-wing UAV can neither move backward directly nor slow down the linear velocity lower than a certain positive value, namely, it is required to maintain a positive minimum airspeed due to the stall conditions.[30] Therefore, different from the traditional unicycle model, the velocity constraints of each fixed-wing UAV are described by a saturated angular velocity and a linear velocity bounded by two positive constants. The leader-follower formation problem for the unicycle-type vehicles was considered in References 31,32, in which a cascaded approach was used to achieve the exponential stability of the closed-loop system. However, the approach cannot be applied to track a leader along straight paths, and this problem was fixed by Loria.[33] Further, an integral sliding-mode control strategy was proposed to eliminate the need for measurement or estimation of the absolute velocity of the leader.[34] Afterwards, a distributed controller for the leader-follower formation was proposed in Reference 35 with the aid of the small-gain method, for the networked unicycle dynamical systems with positive minimum linear velocity constraints. Following this work, a distributed control law was proposed for the leader-follower formation of UAVs subject to both linear and angular velocity constraints in Reference 36. However, the proposed control law in Reference 36 required that the follower UAVs have a wider adjustable range of linear velocity than that of their leaders. In the case where the mobility of the leader is very close to (even the same as) the follower, this method may be inappropriate.

In this paper, we will investigate the leader-follower formation flight control problem of fixed-wing UAVs subject to velocity constraints, that is, the velocity of each UAV is described by a saturated angular velocity and a bounded linear velocity lying between two positive constants. Distributed sliding-mode control laws both for two and more UAVs under directed communication graph are proposed. A nonlinear sliding mode surface is defined for each follower UAV. Using the Lyapunov method, it is proven that the error dynamical system with designed control laws will converge to the sliding mode surface in finite time, and then converge to the origin once it is reaching on the sliding mode surface. It is worthy pointing out that the convergence of the overall system is guaranteed with the condition that the follower UAVs' constraints of both the saturated angular velocity and the bounded linear velocity are satisfied.

The main contributions of the proposed distributed formation control law include:

- The proposed sliding-mode control for leader-follower formation is distributed in the sense that each follower only has access to the information of its leader, and the overall formation is in a network modeled by a tree-like directed graph.
- The desired formation is achieved with the designed control law, and the input constraints of each UAV for both the linear and angular velocities can be always satisfied.
- Compared with the existing works, the leader's speed adjustment range is relaxed in this paper. In the existing works, such as the work in Reference 36, the adjustable range of the followers' linear velocity is required to be larger than that of their leaders' linear velocity. While the speed adjustment range of followers in our method can be the same as that of the leaders'. As a consequence, the whole leader-follower formation system will have a better maneuverability, as its maneuverability is largely determined by that of the leaders. In addition, this relaxation is helpful to construct a "deep" leader- follower system with multiple cascade leaders, because the linear speed adjustment range of the leader can be the same as that of its followers.

The rest of the paper is organized as follows: Section 2 presents some mathematical preliminaries, including the notations problem and some basic control theories. Section 3 gives the problem statement for the distributed leader-follower formation flight of UAVs. In Section 4, a distributed formation control law is proposed and the stability analysis of the

closed-loop system is proved. A numerical simulation as well as the the comparison with the algorithm proposed in Reference 36 are presented in Section 5. Finally, the conclusion is drawn in Section 6.

2 | MATHEMATICAL PRELIMINARIES

We employ $|\cdot|$ to denote the absolute value of a real number. For a vector $x \in \mathbb{R}^n$, its Euclidean norm is represented by $\|x\| = (\sum_{i=1}^{n} |x_i|^2)^{\frac{1}{2}}$ and x^T is its transpose. For a matrix $X \in \mathbb{R}^{m\times n}$, its Euclidean norm is denoted as $\|X\|_F = (\sum_{i=1}^{m}\sum_{j=1}^{n} |x_{ij}|^2)^{\frac{1}{2}}$. For notation simplicity, the subscript F is omitted and $\|\cdot\|$ also denotes the Euclidean norm for a matrix.

A function $\gamma : \mathbb{R}_{\geq 0} \to \mathbb{R}_{\geq 0}$ is positive definite if $\gamma(s) > 0$ for all $s > 0$ and $\gamma(0) = 0$. $\gamma : R_{\geq 0} \to R_{\geq 0}$ is a class $\mathcal{K}$ function if it is continuous, strictly increasing and $\gamma(0) = 0$; it is a class $\mathcal{K}_\infty$ function if it is a class $\mathcal{K}$ function and also satisfies $\gamma(s) \to \infty$ as $s \to \infty$. Supposed $b \leq c$, the saturation function $z = \text{sat}(x, b, c) : \mathbb{R}^3 \to \mathbb{R}$ is defined as

$$z = \text{sat}(x, b, c) = \begin{cases} b, & \text{if } x < b, \\ x, & \text{if } b < x < c, \\ c, & \text{if } x > c. \end{cases} \tag{1}$$

The sign(s) is defined as:

$$\text{sign}(s) = \begin{cases} 1, & s > 0, \\ 0, & s = 0, \\ -1, & s < 0. \end{cases} \tag{2}$$

Definition 1 ([37] Globally Asymptotically Stability). For a system with no inputs $\dot{x} = f(x)$, if there exists a function β of class $\mathcal{KL}$ such that:

$$\|x(t, x^o)\| \leq \beta(\|x^o\|, t), \quad \forall x^o, \forall t \geq 0,$$

then the system is globally asymptotically stable.

Lemma 1 ([37]). *Consider an autonomous system*

$$\dot{x} = f(x), \tag{3}$$

where $f : M \to \mathbb{R}^n$ is a locally Lipschitz map from a domain $M \subset \mathbb{R}^n$ into $\mathbb{R}^n$. Let $x = 0$ be an equilibrium point for (3). Let $V : \mathbb{R}^n \to \mathbb{R}$ be a continuously differentiable function such that:

$$V(0) = 0 \quad \text{and} \quad V(x) > 0, \quad \forall x \neq 0, \tag{4}$$

$$\|x\| \to \infty \Rightarrow V(x) \to \infty, \tag{5}$$

$$\dot{V}(x) < 0, \quad \forall x \neq 0, \tag{6}$$

then $x = 0$ is globally asymptomatically stable.

3 | PROBLEM FORMULATION

Consider a group of N fixed-wing UAVs with kinematic models:

$$\begin{cases} \dot{x}_i = v_i \cos\theta_i, \\ \dot{y}_i = v_i \sin\theta_i, \\ \dot{\theta}_i = \omega_i, \quad i \in [1, N], \end{cases} \tag{7}$$

where x_i and y_i are the position of UAV i in the inertial frame and $\theta_i \in (-\pi, \pi]$ is its heading angle, v_i and ω_i represent the linear velocity and the angular velocity, respectively. In addition, v_i and ω_i are determined by the control inputs $\mu_i = (\mu_i^v, \mu_i^\theta)$, which are

$$\begin{cases} v_i = \mu_i^v, \\ \omega_i = \mu_i^\theta. \end{cases} \tag{8}$$

Further, the following velocity constraints are considered for UAV i:

$$0 < v_i^- < v_i < v_i^+, \tag{9}$$

$$|\omega_i| \leq \omega_i^+, \quad \omega_i^+ > 0, \tag{10}$$

where v_i^- and v_i^+ are the constants which determine the minimum and maximum velocities of the UAV i, respectively, and ω_i^+ is a constant that determines the maximum angular velocity of UAV i.

Remark 1. Compared with the traditional unicycle model, the model of the fixed-wing UAV is additionally constrained by the velocity constraints (9) and (10). Namely, the velocity of each UAV is constrained by a saturated angular velocity and a linear velocity bounded within a positive interval. These constraints make the formation control of UAVs a more challenging problem.

In the leader-follower formation, there is one uncontrolled UAV labeled 0 and this UAV acts as the origin leader of the formation. The other UAVs are followers whose desired trajectories are determined by the origin leader or other follower UAVs. To describe the leader-follower architecture, an acyclic directed graph $\mathcal{G}$ is utilized.

Definition 2 (Formation Control Graph[38]). A formation control graph $\mathcal{F} = (V, E, S)$ is a directed acyclic graph consisting of:

- A finite set $V = \{v_1, \ldots, v_N\}$ of N vertices and a map assigning to each vertex v_i a control system $\dot{\chi}_i = f_i(t, \chi_i, u_i)$ where $\chi_i \in \mathbb{R}^n$.
- An edge set $E \subset V \times V$ encoding leader-follower relationships between vehicles. The ordered pair $(v_i, v_j) \triangleq e_{ij}$ belongs to E if u_j depends on the state of vehicle i, χ_i.
- A collection $D = \{d_{ij}\}$ of edge specifications, defining control objectives (setpoints) for each $j : (v_k, v_j) \in E$ for some $v_i \in V$.

For UAV j, the tail of the incoming edge to vertex j represents the unique leader of UAV j, which is denoted by L_j. Obviously, the origin leader of the whole formation labeled by 0 has no leader, thus $L_0 = \emptyset$. For a vertex j ($1 \leq j \leq N$), we have the following assumption:

Assumption 1. For any vertex $v_j \in V$ ($1 \leq j \leq N$) and its leader vertex L_i, the conditions (9) and (10) always hold. In addition, $[v_i^-, v_i^+] \subseteq [v_j^-, v_j^+]$ and $[\omega_i^-, \omega_i^+] \subset [\omega_j^-, \omega_j^+]$. Meanwhile, there exists an appropriate time interval $[T_1, T_2]$ that the leader's linear speed is smaller than the follower's linear speed, that is, for $\forall t \in [T_1, T_2]$, $v_i(t) < v_j(t)$ holds.

Remark 2. Note that from Assumption 1, the adjustable interval of the linear velocity of the leader can be the same as that of the followers. Actually, Assumption 1 is a relaxed condition compared with the work in Reference 36, which requires the adjustable interval of the linear velocity of the leader should be smaller than that of the followers'. Therefore, under Assumption 1, the maneuverability of the leader can be enhanced to a certain extent, and furthermore, the whole leader-follower formation will have a better maneuverability, as its maneuverability is generally determined by that of its leader.

Through the above definition, a team of UAVs can be represented by a tree-like control graph $\mathcal{G} = \{V, E, D\}$, shown as in Figure 1. The root of the spanning graph is the uncontrolled UAV labeled 0 and is the first class leader of the whole formation. The vertices 1 and 2 are the follower of the vertex 0 while being the leader of the vertices of 3, 4 and 5, 6, respectively. For an ordered pair $(v_i, v_j) \triangleq e_{ij}$ belonging to E, the leader UAV i's position p_i, heading angle θ_i, velocity v_i and angular velocity ω_i can be accessed by the follower UAV j via a perfect communication without delays.

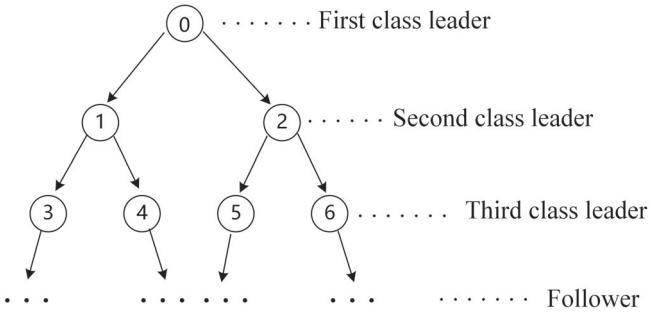

FIGURE 1 A tree-like control graph

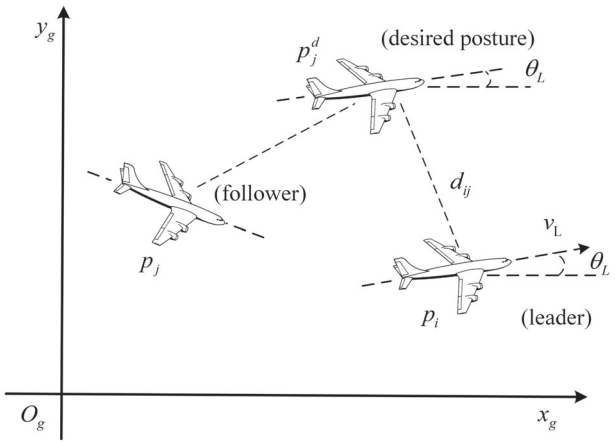

FIGURE 2 Leader-Follower unmanned aerial vehicle formation geometry

As shown in Figure 2, the follower UAV j is expected to keep a preset relative position to its leader UAV i and maintain the same heading angle with the UAV i. If the follower reaches its desired posture with respect to the leader, a desired formation is formed. Let $p_i = (x_i, y_i)$ denote the position of UAV i and θ_i represent its heading angle. Given a specification $d_{ij} = (d_{ij}^x, d_{ij}^y)$ on edge $(v_i, v_j) \in E$, a setpoint for the follower UAV j can be expressed as $p_j^d = p_i - d_{ij}$. Taking the consistence of the heading angle into account, the desired state $\eta_j^d = (x_j^d, y_j^d, \theta_j^d)$ for UAV j is

$$\begin{cases} x_j^d = x_i + d_{ij}^x, \\ y_j^d = y_i + d_{ij}^y, \\ \theta_j^d = \theta_i, \end{cases}$$

where $j \in F_i$. Therefore, the state error $\tilde{\eta}_j = (\tilde{x}_j, \tilde{y}_j, \tilde{\theta}_j)$ of the follower UAV j is defined as

$$\begin{cases} \tilde{x}_j = x_j - x_i - d_{ij}^x, \\ \tilde{y}_j = y_j - y_i - d_{ij}^y, \\ \tilde{\theta}_j = \theta_j - \theta_i. \end{cases} \tag{11}$$

Extending the state error defined by (11) to the whole formation, the formation error vector is constructed by stacking the errors of all followers:

$$\tilde{\eta} \triangleq \left[\dots \tilde{\eta}_j \dots \right]^T, \quad j \in [1, N_{|E|}], \tag{12}$$

where $N_{|E|}$ is the number of edges in graph $\mathcal{G}$. Then, the objective of this paper is to design a controller for each follower UAV to make the stack error $\tilde{\eta}$ converge to the origin.

4 | MAIN RESULTS

To simplify the problem, the tracking control problem for only one pair of leader and follower is considered firstly, and then it is extended to the formation tracking case in the general case.

4.1 | Leader-Follower Tracking Control

Consider a pair of fixed-wing UAVs in which one acts as the leader and the other acts as the follower. For the reading convenience, let (x_F, y_F, θ_F) and (x_L, y_L, θ_L) denote the planar coordination and the heading angle of the follower and the leader UAV in the inertial frame, respectively. Then (11) in this case becomes:

$$\begin{cases} \tilde{x}_F = x_F - x_L - d_{LF}^x, \\ \tilde{y}_F = y_F - y_L - d_{LF}^y, \\ \tilde{\theta}_F = \theta_F - \theta_L, \end{cases} \tag{13}$$

where (d_{LF}^x, d_{LF}^y) is the desired relative position between the leader UAV and the follower UAV. Meanwhile, the follower UAV obeys the following velocity constraints:

$$0 < v_{\min} \le v_F \le v_{\max}, \tag{14}$$

$$0 \le |\omega_F| \le \omega_{\max}, \quad \omega_{\max} > 0, \tag{15}$$

where $\omega_{\max}$ is the maximum angular velocity of the follower UAV, $v_{\min}$ and $v_{\max}$ are, respectively, the minimum and maximum linear velocities of the follower UAV.

A leader-aligned coordinate called $\mathcal{D}$-coordinate is firstly defined. As illustrated in Figure 3, the frame $O_g x_g y_g$ is the inertial frame and the origin of $\mathcal{D}$-coordinate $(O_D x_D y_D)$ is fixed with the desired position of the follower UAV and its x-coordinate is consistent with the heading direction of the leader UAV. Based on this, a coordinate transformation is performed as follows:

$$\begin{bmatrix} x_e \\ y_e \\ \theta_e \end{bmatrix} = \begin{bmatrix} \cos\theta_L & \sin\theta_L & 0 \\ -\sin\theta_L & \cos\theta_L & 0 \\ 0 & 0 & 1 \end{bmatrix} \begin{bmatrix} \tilde{x}_F \\ \tilde{y}_F \\ \tilde{\theta}_F \end{bmatrix}, \tag{16}$$

where (x_e, y_e, θ_e) is the tracking error in the $\mathcal{D}$-coordinate and $\theta_e \in (-2\pi, 2\pi)$. By performing the transformation (11) and (16), the position of the follower is transferred from the world-coordinate into the $\mathcal{D}$-coordinate. In the new coordinate, the error dynamics between the leader and the follower becomes

$$\begin{cases} \dot{x}_e = \omega_L y_e - v_L + v_F \cos\theta_e, \\ \dot{y}_e = -\omega_L x_e + v_F \sin\theta_e, \\ \dot{\theta}_e = \omega_F - \omega_L. \end{cases} \tag{17}$$

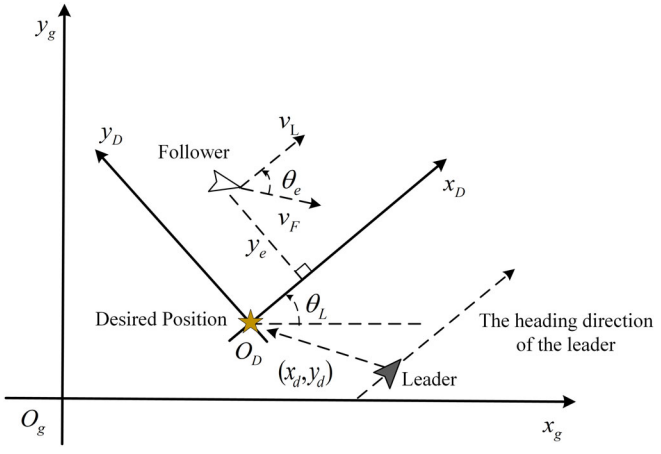

FIGURE 3 The illustration of two coordinates: world-coordinate and $\mathcal{D}$-coordinate [Colour figure can be viewed at wileyonlinelibrary.com]

A control law $\mu = (\mu_F^v, \mu_F^\theta)$ that enforces the trajectory of (17) to be globally stable is to be designed. In the following part, we design a sliding mode controller which guarantees the global stabilization of the system (17). Firstly define the sliding mode surface s as

$$s = \theta_e + k_1 \frac{y_e}{k_2 + r_e}, \tag{18}$$

where $r_e = \sqrt{x_e^2 + y_e^2}$ and k_1, k_2 are constants. Then a controller is designed as

$$\mu_F^v = \begin{cases} sat\left(\frac{v_L - k_3 x_e}{\cos\theta_e}, v_{\min}, v_{\max}\right), & if\ |\theta_e| \neq \frac{\pi}{2}, \frac{3\pi}{2}, \\ v_{\max}, & if\ |\theta_e| = \frac{\pi}{2}, \frac{3\pi}{2}, \end{cases} \tag{19}$$

$$\mu_F^\theta = -\left(k_1 \frac{(v_L x_e - v_F \cos\theta_e x_e - v_F \sin\theta_e y_e) y_e}{r_e (k_2 + r_e)^2} + k_1 \frac{v_F \sin\theta_e - \omega_L x_e}{k_2 + r_e} + k_4 \text{sign}(s)\right) + \omega_L, \tag{20}$$

where k_3 and k_4 are the coefficient constants and the functions sat$(\cdot)$ and sign$(\cdot)$ are defined in (1) and (2), respectively.

Let v_L^+ and w_L^+ denote the maximum linear velocity and maximum angular velocity of the leader, respectively, and the stability proof of the system (17) with controller (19) and (20) is provided in the following theorem:

Theorem 1. *Consider the system (17) under the controller (19) and (20). If the parameters k_1, k_2, k_3, and k_4 satisfy the following conditions:*

$$0 < k_1 < \frac{4}{\pi^2}, \tag{21}$$

$$k_2 > k_1 \frac{v_L^+ + 2v_{\max}}{\omega_{\max} - k_4 - (k_1 + 1) w_L^+} > 0, \tag{22}$$

$$k_3 > 0, \quad and \quad k_4 > 0, \tag{23}$$

then the closed-loop system (17) will converge to the origin and the velocity constraints (14) and (15) are satisfied.

Proof. Firstly, we will prove that the system will globally converge to the slide mode surface $s = 0$ defined in (18) in finite time from any initial states, driven by control law (19) and (20). Define a Lyapunov function candidate as

$$V_s = \frac{1}{2} s^2.$$

Then, the time derivative of V_s is

$$\begin{aligned} \dot{V}_s = s\dot{s} &= s\left(\dot{\theta}_e - k_1 \frac{\dot{r}_e y_e}{(k_2 + r_e)^2} + k_1 \frac{\dot{y}_e}{k_2 + r_e}\right) \\ &= s\left(\dot{\theta}_e - k_1 \frac{y_e}{(k_2 + r_e)^2} \cdot \frac{-v_L x_e + v_F \cos\theta_e x_e + v_F \sin\theta_e y_e}{r_e} + k_1 \frac{-\omega_L x_e + v_F \sin\theta_e}{k_2 + r_e}\right). \end{aligned} \tag{24}$$

Note that here $\dot{\theta}_e = \omega_F - \omega_L = \mu_F^\theta - \omega_L$, where μ_F^θ is the designed controller defined in (20). As a consequence, we have

$$\dot{V}_s = -k_4 s \cdot \text{sign}(s) = -k_4 |s| \leq 0. \tag{25}$$

The equality is achieved if and only if $s = 0$.

Denote $W = \sqrt{2V_s} = |s|$, and the right differential D^+W of W satisfies the differential inequality:

$$D^+ W \leq -k_4.$$

Then the comparison lemma[37] shows that

$$W(s(t)) \leq W(s(0)) - k_4 t. \tag{26}$$

Therefore, the trajectory reaches the manifold $s = 0$ in finite time, and, once on the manifold $s = 0$, it cannot leave it, as seen from the inequality $\dot{V}_s \leq -k_4|s|$.

Next the convergence of the system on the sliding mode surface $s = 0$ will be analyzed. Recall the sliding mode surface (18). When $s = 0$, it yields

$$\theta_e = -\frac{k_1}{k_2 + r_e} y_e. \tag{27}$$

Obviously, θ_e will also converge to 0 when $y_e \to 0$. Thus the convergence of θ_e is guaranteed as long as the convergence of y_e is ensured.

Define a Lyapunov function candidate as

$$V = \frac{1}{2}x_e^2 + \frac{1}{2}y_e^2. \tag{28}$$

When $s = 0$, it can be obtained from (27) that

$$y_e = -\frac{k_2 + r_e}{k_1}\theta_e. \tag{29}$$

Then combined with (17) and (29), the time derivative of V yields

$$\begin{aligned}
\dot{V} &= x_e\dot{x}_e + y_e\dot{y}_e \\
&= (v_F \cos\theta_e - v_L)x_e + v_F \sin\theta_e y_e \\
&= (v_F \cos\theta_e - v_L)x_e + v_F \sin\theta_e \left(-\frac{k_2 + r_e}{k_1}\theta_e\right) \\
&\leq (v_F \cos\theta_e - v_L)x_e - \frac{k_2 + r_e}{k_1} v_F \theta_e^2.
\end{aligned} \tag{30}$$

Firstly, when $\cos\theta_e = 0$, that is,$|\theta_e| = \pi/2$ or $|\theta_e| = 3\pi/2$, we have $\theta_e^2 \geq \pi^2/4$ and can further deduce the following inequality:

$$\begin{aligned}
\dot{V} &\leq -\frac{k_2}{k_1} v_F \theta_e^2 + v_{\max}\left(|x_e| - \frac{\pi^2 r_e}{4k_1}\right) \\
&\leq -\frac{k_2}{k_1} v_F \theta_e^2 + v_{\max}|x_e|\left(1 - \frac{\pi^2}{4k_1}\right).
\end{aligned}$$

As $k_1 < 4/\pi^2$ revealed by the condition (21), it holds that $(1 - \pi^2/(4k_1)) < 0$, which yields

$$\dot{V} < -\frac{k_2}{k_1} v_F |\theta_e|^2 - v_{\max}\left|1 - \frac{\pi^2}{4k_1}\right| |x_e| < 0. \tag{31}$$

Then, when $\cos\theta_e \neq 0$ and the desired velocity v_F is within the allowed range, that is, $v_{\min} \leq v_F = \frac{v_L - k_3 x_e}{\cos\theta_e} \leq v_{\max}$, (30) becomes

$$\dot{V} \leq -k_3 x_e^2 - \frac{k_2 + r_e}{k_1} v_F \theta_e^2 \leq 0. \tag{32}$$

The equality in (32) holds if and only if $x_e = 0$ and $\theta_e = 0$, which further leads to the global stability of the system in this case.

On the other hand, when $\cos\theta_e \neq 0$ and the desired velocity v_F is limited by the velocity saturation, there are 8 cases listed as follows:

(1) $\frac{v_L - k_3 x_e}{\cos\theta_e} > v_{\max}, \cos\theta_e > 0, x_e \geq 0, v_F = v_{\max}$;

(2) $\frac{v_L - k_3 x_e}{\cos\theta_e} > v_{\max}, \cos\theta_e > 0, x_e < 0, v_F = v_{\max}$;

(3) $\frac{v_L - k_3 x_e}{\cos\theta_e} > v_{\max}, \cos\theta_e < 0, x_e \geq 0, v_F = v_{\max}$;

(4) $\frac{v_L - k_3 x_e}{\cos\theta_e} > v_{\max}, \cos\theta_e < 0, x_e < 0, v_F = v_{\max}$;

(5) $\frac{v_L - k_3 x_e}{\cos\theta_e} < v_{\min}, \cos\theta_e > 0, x_e \geq 0, v_F = v_{\min}$;

(6) $\frac{v_L - k_3 x_e}{\cos\theta_e} < v_{\min}, \cos\theta_e > 0, x_e < 0, v_F = v_{\min}$;

(7) $\frac{v_L - k_3 x_e}{\cos\theta_e} < v_{\min}, \cos\theta_e < 0, x_e \geq 0, v_F = v_{\min}$;

(8) $\frac{v_L - k_3 x_e}{\cos\theta_e} < v_{\min}, \cos\theta_e > 0, x_e < 0, v_F = v_{\min}$.

It is easy to verify that cases (4) and (8) are impossible. Therefore, we will discuss the rest cases in the following part.

- For cases (1) and (6), we have

$$-v_L x_e < -k_3 x_e^2 - v_F \cos\theta_e x_e. \tag{33}$$

Substituting (33) into (30) gives(32).

- For cases (3), (5), and (7), it is clear that $x_e > 0$ holds in these cases. Considering $(v_F \cos\theta_e - v_L) < 0$, it yields

$$\dot{V} \leq -|v_F \cos\theta_e - v_L||x_e| - \frac{k_2 + r_e}{k_1} v_F \theta_e^2 \leq 0. \tag{34}$$

Obviously, the equality in (34) holds also only when $x_e = 0$ and $\theta_e = 0$.

- For case (2), substituting $v_F = v_{\max}$ into (30) yields

$$\begin{aligned}
\dot{V} &\leq -\frac{k_2}{k_1} v_{\max}\theta_e^2 + (v_L - v_{\max}\cos\theta_e)|x_e| - \frac{r_e}{k_1} v_{\max}\theta_e^2 \\
&\leq -\frac{k_2}{k_1} v_{\max}\theta_e^2 + \left(v_{\max} - v_{\max}\cos\theta_e - \frac{v_{\max}}{k_1}\theta_e^2\right)|x_e| \\
&= -\frac{k_2}{k_1} v_{\max}\theta_e^2 + \left(1 - \cos\theta_e - \frac{1}{k_1}\theta_e^2\right)|x_e| v_{\max}.
\end{aligned} \tag{35}$$

Note that

$$1 - \cos\theta_e = 2\sin^2\frac{\theta_e}{2} \leq \frac{\theta_e^2}{2}. \tag{36}$$

Substituting (36) into (35) yields

$$\dot{V} \leq -\frac{k_2}{k_1} v_{\max}\theta_e^2 - \left(\frac{1}{k_1} - \frac{1}{2}\right) v_{\max}\theta_e^2 |x_e|. \tag{37}$$

Note that $k_1 < 4/\pi^2 < 2$, thus $1/k_1 - 1/2 > 0$. Further from (37), it can be observed that $\dot{V} < 0$ as long as $\theta_e \neq 0$. According to Assumption 1, $|v_L| \leq v_L^+ \leq v_{\max}$, where v_L^+ is the maximum velocity of the leader. Further when $\theta_e = 0$, (30) can be written as

$$\dot{V} = (v_{\max} - v_L)x_e = -|v_{\max} - v_L||x_e|. \tag{38}$$

From (38), it can be induced that $\dot{V} \leq 0$ holds as well and the equality holds only if $x_e = 0$. Thus combining (37) with (38), it can be concluded that $\dot{V} < 0$ as long as $\theta_e \neq 0$ and $y_e \neq 0$ for the case 2).

From (27), it is known that $\theta_e \neq 0$ if $y_e \neq 0$. Therefore, when $s = 0$, it always holds that $\dot{V} \leq 0$ and the equality holds if and only if $x_e = 0$ and $y_e = 0$ through the discussions above. Following that, it can be concluded from Lemma 1 that x_e and y_e will converge to the origin when $s = 0$. Together with the result that the manifold $s = 0$ can be reached in finite time, we can conclude that the closed-loop system (17) under the controller (19) and (20) is globally stable. ∎

The boundedness of the input will be analyzed. Firstly, the velocity constraint that $v_{min} \leq v_F \leq v_{max}$ holds obviously. Then, for the angular velocity input μ_F^θ, define $\phi = a\tan 2(y_e, x_e)$ and we have

$$\begin{aligned}
|\mu_F^\theta| &\leq k_1 \left| \frac{-v_L x_e + v_F \cos\theta_e x_e + v_F \sin\theta_e y_e}{r_e(r_e + k_2)} \right| + k_1 \left| \frac{-\omega_L x_e + v_F \sin\theta_e}{r_e + k_2} \right| + |\mu_L^\theta| + k_4 \\
&\leq \frac{k_1}{r_e + k_2}(|v_L| + |v_F \cos\theta_e \cos\phi + v_F \sin\theta_e \sin\phi|) + k_1 \left(|\omega_L| + \frac{|v_F \sin\theta_e|}{r_e + k_2} \right) + |\mu_L^\theta| \\
&\leq \frac{k_1}{r_e + k_2}(|v_L| + |v_F \cos(\theta_e - \phi)| + |v_F|) + k_1|\omega_L| + |\mu_L^\theta| + k_4 \\
&\leq \frac{k_1}{k_2}(v_L^+ + 2v_{\max}) + (k_1 + 1)w_L^+ + k_4.
\end{aligned} \tag{39}$$

By substituting the condition (22) into (39), we obtain $|\mu_F^\theta| \leq \omega_{\max}$.

Remark 3. The parameter k_3 is related with the convergence rate of x_e. In general, a larger k_3 will bring a faster convergence of x_e. The parameter k_1 is related with the convergence rate of y_e and an excessively small k_1 will incur a slow convergence of y_e. In order to keep k_1 not to be excessively small while the condition (22) is satisfied, the parameter k_2 could be relatively large.

Remark 4. It should be noted that the chattering may happen at the neighborhood of the equilibrium $s = 0$ because of the signum function *sign*(*s*). In order to avoid the chattering in practice, the function sign(*s*) defined in (2) can be replaced with other "softer" functions, such as the tangent function $\tanh(s/\varepsilon)$ or a continuous function $\frac{s}{|s|+\varepsilon}$, where ε is a positive number selected to reduce the chattering problem. For more details, please refer to Reference 37.

Remark 5. From Theorem 1, the formation control law composed of (18), (19), and (20) guarantees the stability of the closed-loop leader-follower system while the velocity constraints are satisfied. Namely, the proposed control law can still work well even when the adjustable range of the leader's linear velocity is the same as that of the followers', which is different from the previous work. In order to guarantee the stability of the overall system, the parameters in Reference 36 is quite conservative when the adjustable range of the leader's linear velocity approaches that of the follower's, and the performance may be not so good in this case. From the proof of Theorem 1, it can be inferred that the proposed algorithm can still work well as long as there exists a time interval that the leader's speed is smaller than that of the followers.

4.2 | Leader-Follower Formation Control

Now, we extend the previous result to the case of formation tracking control. For a given ordered pair $(v_j, v_i) \triangleq e_{ji}$ belonging to E, define the error vector $\eta_{ei} = (x_{ei}, y_{ei}, \theta_{ei})$, which is the extension of (16) as follows:

$$\begin{bmatrix} x_{ei} \\ y_{ei} \\ \theta_{ei} \end{bmatrix} = \begin{bmatrix} \cos\theta_j & \sin\theta_j & 0 \\ -\sin\theta_j & \cos\theta_j & 0 \\ 0 & 0 & 1 \end{bmatrix} \begin{bmatrix} \tilde{x}_i \\ \tilde{y}_i \\ \tilde{\theta}_i \end{bmatrix}. \tag{40}$$

Then similar to (17), the dynamics of error η_{ei} becomes

$$\begin{cases} \dot{x}_{ei} = \omega_j y_{ei} - v_j + v_i \cos\theta_{ei}, \\ \dot{y}_{ei} = -\omega_j x_{ei} + v_i \sin\theta_{ei}, \\ \dot{\theta}_{ei} = \omega_i - \omega_j. \end{cases} \tag{41}$$

A sliding mode surface for UAV i is defined as

$$s_i = \theta_{ei} + k_1 \frac{y_{ei}}{k_2 + r_{ei}}, \tag{42}$$

where $r_{ei} = \sqrt{x_{ei}^2 + y_{ei}^2}$. Then, the distributed sliding mode controller for UAV i is proposed as

$$\mu_i^v = \begin{cases} sat\left(\frac{v_j - k_3 x_{ei}}{\cos\theta_{ei}}, v_i^-, v_i^+\right), & if\ |\theta_{ei}| \neq \frac{\pi}{2}, \frac{3\pi}{2}, \\ v_i^+, & if\ |\theta_{ei}| = \frac{\pi}{2}, \frac{3\pi}{2}, \end{cases} \tag{43}$$

$$\mu_i^\theta = -\left(k_1 \frac{(v_j x_{ei} - v_i \cos\theta_{ei} x_{ei} - v_i \sin\theta_{ei} y_{ei}) y_{ei}}{r_{ei}(k_2 + r_{ei})^2} + k_1 \frac{v_i \sin\theta_{ei} - \omega_j x_{ei}}{k_2 + r_{ei}} + k_4 \text{sign}(s_i)\right) + \omega_j, \tag{44}$$

where $j = L_i$, and k_1, k_2, k_3, k_4 are constants and satisfies

$$0 < k_1 < \frac{4}{\pi^2}, \tag{45}$$

$$k_2 > k_1 \frac{v_j^+ + 2v_i^+}{\omega_i^+ - k_4 - (k_1 + 1)w_j^+} > 0, \tag{46}$$

$$k_3 > 0, \quad k_4 > 0. \tag{47}$$

Now it is the position to present the formation controller.

Theorem 2. *Consider the formation of N UAVs whose kinematic model is given by (7) and the communication relationship is determined by a tree-like digraph $\mathcal{G}$, the error dynamics for any pair of two connected UAVs is given by (41). Given the distributed sliding mode control law (42), (43), and (44), the convergence of the formation error $\tilde{\eta}$ defined by (11) and (12) to the origin can be guaranteed.*

Proof. Define a Lyapunov function V_{si} for each UAV i as

$$V_{si} = \frac{1}{2} s_i^2. \tag{48}$$

It can be concluded using the method similar to the proof of Theorem 1 that

$$V_{si} = -k_4 |s_i| \leq 0, \tag{49}$$

and the trajectory of s_i will reach the manifold $s_i = 0$ in finite time. By using a similar method in Theorem 1, it can be proved that the system (41) driven by the control law (43) and (44) will asymptotically converge to the origin in finite time if $s_i = 0$. Let T_i denote the time when s_i reaches the manifold $s_i = 0$. Combining with the definition of the globally asymptotically stability in Definition 1 yields

$$\|\eta_{ei}(t)\| \leq \beta_i(\|\eta_{ei}(T_i)\|, t), \quad \forall t \geq T_i, \tag{50}$$

where β_i is a class $\mathcal{KL}$ function. Since $\|\tilde{\eta}_i(t)\| = \|\eta_{ei}(t)\|$, we have

$$\|\tilde{\eta}_i(t)\| \leq \beta_i(\|\tilde{\eta}_i(T_i)\|, t), \quad \forall t \geq T_i. \tag{51}$$

Denoting $T_{\max} = \max_{1 \leq i \leq N} \{T_i\}$ and summing over all $1 \leq i \leq N$, we obtain that

$$\begin{aligned} \|\tilde{\eta}(t)\| &\leq \sum_{i=1}^{N} \|\tilde{\eta}_i(t)\| \leq \sum_{i=1}^{N} \beta_i(\|\tilde{\eta}_i(T_{\max})\|, t) \\ &\leq \sum_{i=1}^{N} \beta_i(\|\tilde{\eta}(T_{max})\|, t), \quad \forall t \geq T_{max}. \end{aligned} \tag{52}$$

As $\beta_i(\cdot)$ is a class $\mathcal{KL}$ function, $\beta_i(\|\tilde{\eta}(T_{max})\|, t) \to 0$ when $t \to \infty$. Thus, it can be induced from (52) that $\|\tilde{\eta}(t)\| \to 0$ when $t \to \infty$. The proof is completed. ∎

Remark 6. It is clear that the proposed control law composing of (42), (43) and (44) only uses its own information and the information of its leader UAV, which is distributed and scalable. In addition, the control law is of significance for a "deep"' leader-follower systems with multiple cascade leaders, as shown in Figure 1, because the follower's speed adjustment range can be the same as that of the leader. If the adjustable range of the followers' linear velocity is required to be strictly larger than their leaders', the velocity adjustable range of the followers in the "deeper" class has to be larger and larger. This is the reason why it is hard to construct a "deep" leader- follower system.

5 | SIMULATION RESULTS

In this section, two simulation scenarios are presented. In the first simulation, the case of only a pair of leader and follower is considered. and in the second simulation, a formation consisting of a leader UAV and six follower UAVs is investigated.

In the first case, the reference path of the leader UAV is a sinusoidal-like curve. The follower is expected to keep a relative position $(40, 40)$ from the leader. The initial positions of the leader and the follower are given by $[30, 40]$ and $[-300, -300]$, respectively. The velocity constraint for the follower UAV in the simulation is given as $v_F \in [12, 20]$. The maximum angular velocity for the follower is 1.2 rad/s. The linear velocity and the angular velocity of the leader robot are given as $v_L(t) = (15 - \cos 0.2t)$ m/s and $\omega_L(t) = 0.1 \cos 0.2t$. Therefore, the leader's velocity is constrained by $v_L \subseteq [14, 16]$.

The parameters in the designed control law (19) and (20) are given by $k_1 = 0.4$, $k_2 = 30$, $k_3 = 1$ and $k_4 = 0.2$. Further, we compare the proposed algorithm with the algorithm in,[36] which is explicitly described as follows:

$$\begin{aligned} v_F &= v_L + \frac{\hat{k}_1 \hat{x}_e}{\sqrt{1 + \hat{x}_e^2 + \hat{y}_e^2}}, \\ \omega_F &= \omega_L + \frac{\hat{k}_3 \sin \frac{\hat{\theta}_{ei}}{2}}{\sqrt{1 + \hat{x}_{ei}^2 + \hat{y}_{ei}^2}} + \frac{\hat{k}_2 \text{sat}\left(v_F, v_L^+, v_L^-\right)\left(\hat{y}_{ei} \cos \frac{\hat{\theta}_{ei}}{2} - \hat{x}_{ei} \sin \frac{\hat{\theta}_{ei}}{2}\right)}{\sqrt{1 + \hat{x}_{ei}^2 + \hat{y}_{ei}^2}}, \end{aligned} \tag{53}$$

where $\hat{x}_e, \hat{y}_e, \hat{\theta}_e$ are given by

$$\begin{bmatrix} \hat{x}_e \\ \hat{y}_e \\ \hat{\theta}_e \end{bmatrix} = \begin{bmatrix} -\cos\theta_L & \sin\theta_L & 0 \\ \sin\theta_L & -\cos\theta_L & 0 \\ 0 & 0 & -1 \end{bmatrix} \begin{bmatrix} \tilde{x}_F \\ \tilde{y}_F \\ \tilde{\theta}_F \end{bmatrix}, \tag{54}$$

$\hat{k}_1$, $\hat{k}_2$, and $\hat{k}_3$ are coefficient constants and satisfy

$$\begin{aligned} &\hat{k}_1 \le \min\left(v_{\max} - v_L^+, v_L^- - v_{\min}\right), \\ &2\hat{k}_2 v_L^+ + \hat{k}_3 \le \omega_{\max} - \omega_L^+. \end{aligned} \tag{55}$$

Constrained by (55), the parameter $\hat{k}_1$ in (53) should satisfy $\hat{k}_1 \le 2$. Thus choose the parameters in (53) as $\hat{k}_1 = 2$, $\hat{k}_2 = 0.008$, $\hat{k}_3 = 0.25$.

The paths of the follower controlled by our algorithm and the algorithm in[36] as well as the leader's path are illustrated in Figure 4A. The tracking errors x_e, y_e, θ_e are compared in Figure 4B, Figure 4C, and Figure 4D, respectively. The angular speed and velocity of the UAVs controlled by two methods are shown in Figure 5. It can be observed from Figure 5B that the velocity of the UAV controlled by our algorithm can reach the maximum speed 20m/s at the beginning of the simulation. On the contrary, the UAV controlled by the algorithm in Reference 36 cannot reach the maximum performance speed of airplane because the parameter k_1 is limited by $k_1 \le v_L^- - v_{\min} = 2$. Therefore, if the UAV is controlled by the algorithm in Reference 36, the velocity of the follower UAV is constrained by $v_F \le v_L + \hat{k}_1 = 18$m/s. As a consequence, the tracking error x_e of the algorithm in Reference 36 converges much slower than that of our algorithm, which is illustrated in Figure 4B. Figure 5A shows that the angular speed of both algorithm is within the allowed range.

In the second simulation, we consider a formation consisting of a leader UAV (labeled 0) and six follower UAVs (labeled $1 - 6$) with kinematics (1). The desired formation shape is a triangle. The communication topology as well as the desired relative position inside the formation is shown in Figure 6. The velocity of the leader for the formation is given by $v_0 = 16 - 4\sin(0.1\pi t)$ and thus $v_0 \in [12, 20]$. The adjustable range of the followers' velocity is just the same as that of the leader

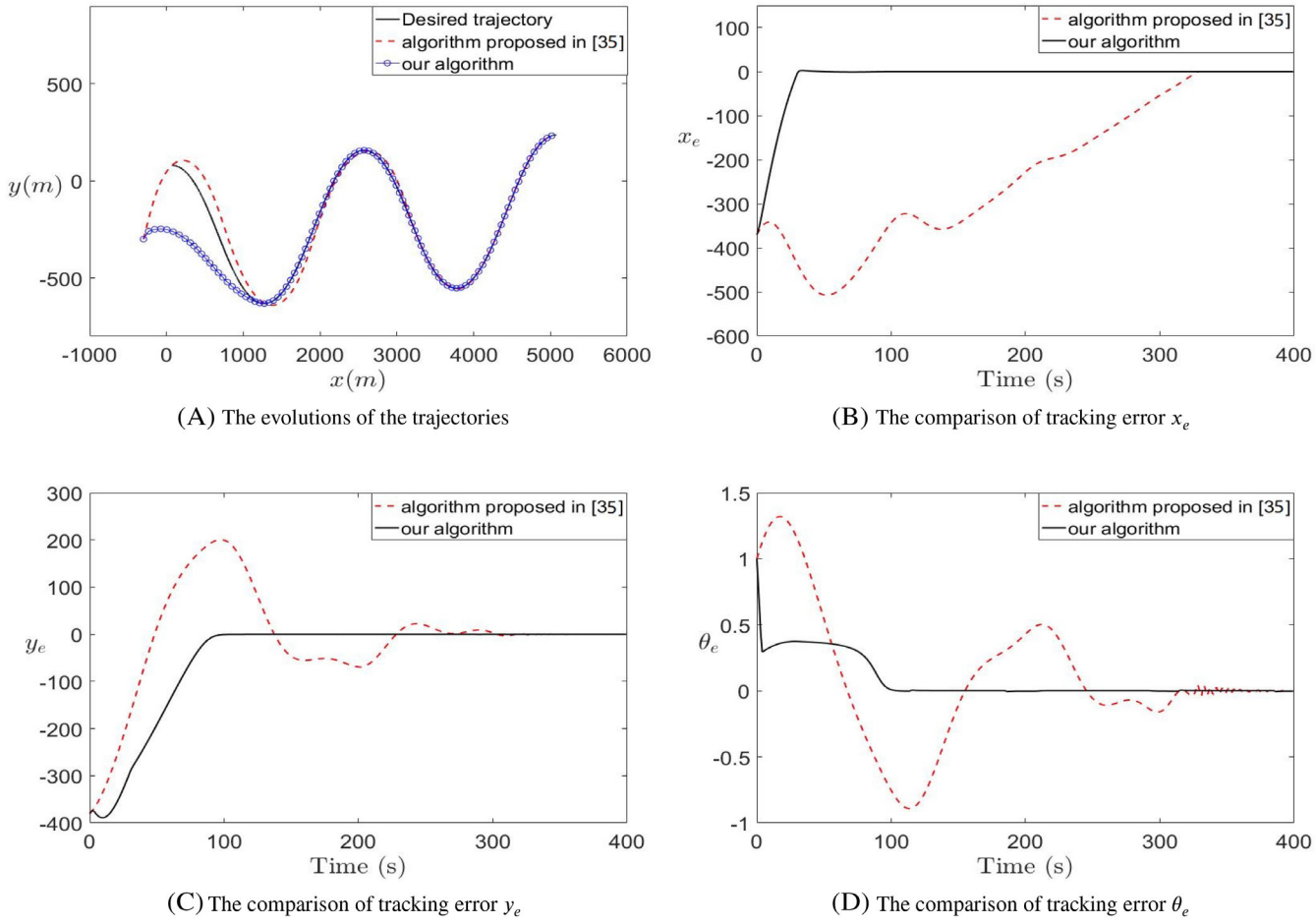

(A) The evolutions of the trajectories

(B) The comparison of tracking error x_e

(C) The comparison of tracking error y_e

(D) The comparison of tracking error θ_e

FIGURE 4 Described paths and the comparison of tracking errors controlled by two methods [Colour figure can be viewed at wileyonlinelibrary.com]

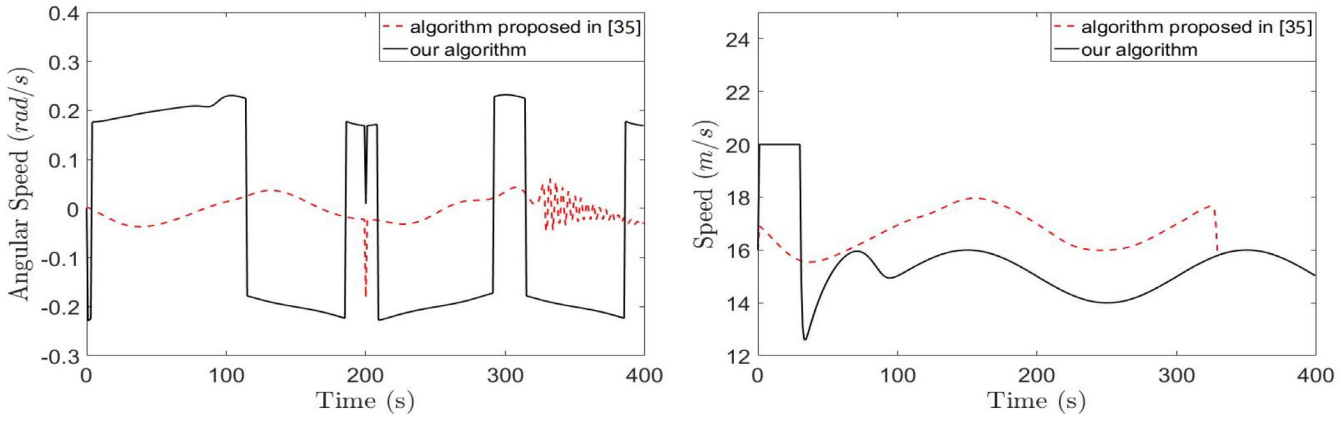

(A) The comparison of angular speed

(B) The comparison of velocity

FIGURE 5 The illustration of the follower's speed and angular speed controlled by two methods [Colour figure can be viewed at wileyonlinelibrary.com]

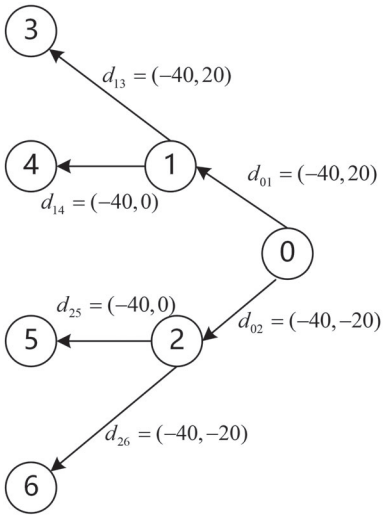

FIGURE 6 The illustration of the desired formation in the simulation

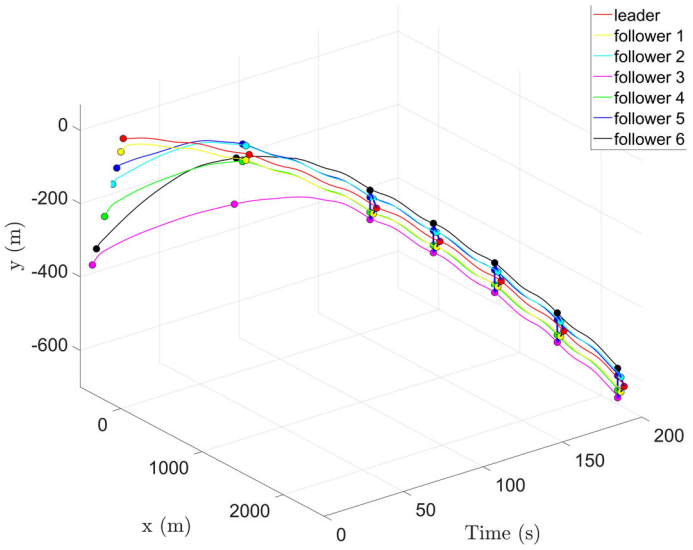

FIGURE 7 Trajectories of the leader unmanned aerial vehicle (UAV) and all follower UAVs [Colour figure can be viewed at wileyonlinelibrary.com]

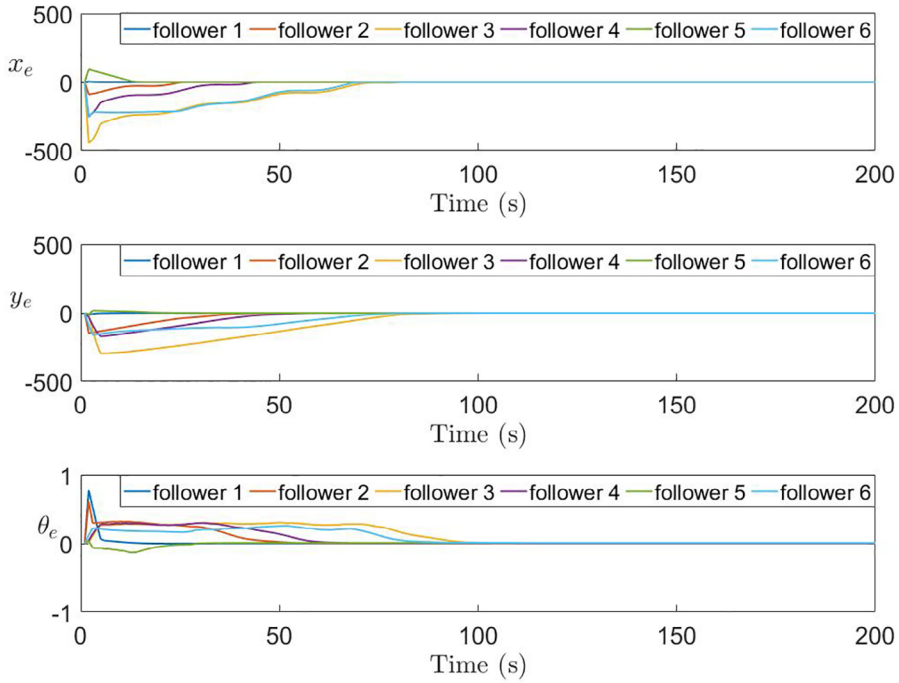

FIGURE 8 Formation tracking errors of each follower unmanned aerial vehicle [Colour figure can be viewed at wileyonlinelibrary.com]

vehicle, i.e., $v_i \in [12, 20]$, $i = 1, 2, \dots, 6$. The control parameters in this case are the same as those in the first simulation. Figure 7 shows the trajectories of all UAVs during the simulation of 200*s*. The positions of all the UAVs at certain moments during the simulation are marked by solid balls. It can be observed that the UAV formation converges to the desired triangle shape. The tracking errors x_e, y_e, θ_e of all follower UAVs are shown in Figure 8, which shows that the formation tracking errors will converge to 0. The simulation results verify the effectiveness of the control law proposed in this paper and prove that our algorithm can still work well even when the the adjustable range of the followers' velocity is just the same as that of the leader's.

6 | CONCLUSION

In this paper, a distributed sliding-mode control law has been proposed for fixed-wing UAVs formation flight subject to velocity constraints. Driven by the proposed control law, the linear velocity of each follower is guaranteed to lie between two positive constants while the desired leader-follower formation is achieved. In addition, the adjustable range of the followers' linear velocity is not required to be larger than that of the leader's, which is of significance in the leader-follower formation flight for a large scale of UAVs.

Although we relax the limit on the adjustable range of the follower's linear velocity, the maximum angular velocity of the follower is still required to be larger than its leader. This may limit its applications to the formation flight for a large scale of UAVs. Besides, the collision between the UAVs will be considered in future.

ORCID

Xiangke Wang https://orcid.org/0000-0002-5074-7052

REFERENCES

1. Gupta SG, Ghonge MM, Jawandhiya P. Review of unmanned aircraft system (UAS). *Int J Adv Res Comput Eng Tech*. 2013;2(4):1646-1658.
2. Mohamed A, El-Gindy M, Ren J. Advanced control techniques for unmanned ground vehicle: literature survey. *Int J Veh Perform*. 2018;4(1):46-73.
3. Liu Z, Zhang Y, Yu X, Yuan C. Unmanned surface vehicles: an overview of developments and challenges. *Ann Rev Control*. 2016;41:71-93.
4. Liu P, Chen AY, Huang YN, et al. A review of rotorcraft unmanned aerial vehicle (UAV) developments and applications in civil engineering. *Smart Struct Syst*. 2014;13(6):1065-1094.
5. Wang X, Shen L, Liu Z, et al. Coordinated flight control of miniature fixed-wing UAV swarms: methods and experiments. *Sci China Inf Sci*. 2019;62(11):212204.
6. Wang X, Zeng Z, Cong Y. Multi-agent distributed coordination control: developments and directions via graph viewpoint. *Neurocomputing*. 2016;199:204-218.
7. Oh KK, Park MC, Ahn HS. A survey of multi-agent formation control. *Automatica*. 2015;53:424-440.
8. Cao Y, Yu W, Ren W, Chen G. An overview of recent progress in the study of distributed multi-agent coordination. *IEEE Trans Ind Inform*. 2013;9(1):427-443.
9. Desai JP, Ostrowski JP, Kumar V. Modeling and control of formations of nonholonomic mobile robots. *IEEE Trans Robot Automat*. 2001;17(6):905-908.
10. Gustavi T, Hu X. Observer-based leader-following formation control using onboard sensor information. *IEEE Trans Robot*. 2008;24(6):1457-1462.
11. Antonelli G, Arrichiello F, Chiaverini S. The entrapment/escorting mission for a multi-robot system: theory and experiments. Paper presented at: Proceedings of the IEEE/ASME International Conference on Advanced Intelligent Mechatronics; 2007:1-6.
12. Lawton JR, Beard RW, Young BJ. A decentralized approach to formation maneuvers. *IEEE Trans Robot Automat*. 2003;19(6):933-941.
13. Yang T, Roy S, Wan Y, Saberi A. Constructing consensus controllers for networks with identical general linear agents. *Int J Robust Nonlinear Control*. 2011;21(11):1237-1256.
14. Yang T, Meng Z, Dimarogonas DV, Johansson KH. Global consensus for discrete-time multi-agent systems with input saturation constraints. *Automatica*. 2014;50(2):499-506.
15. Das AK, Fierro R, Kumar V, Ostrowski JP, Spletzer J, Taylor CJ. A vision-based formation control framework. *IEEE Trans Robot Automat*. 2002;18(5):813-825.
16. Consolini L, Morbidi F, Prattichizzo D, Tosques M. Leader–follower formation control of nonholonomic mobile robots with input constraints. *Automatica*. 2008;44(5):1343-1349.
17. Ji Z, Wang Z, Lin H, Wang Z. Interconnection topologies for multi-agent coordination under leader–follower framework. *Automatica*. 2009;45(12):2857-2863.
18. Hu J, Feng G. Distributed tracking control of leader–follower multi-agent systems under noisy measurement. *Automatica*. 2010;46(8):1382-1387.

19. Hong Y, Wang X, Jiang ZP. Distributed output regulation of leader–follower multi-agent systems. *Int J Robust Nonlinear Control*. 2013;23(1):48-66.
20. Chen J, Sun D, Yang J, Chen H. Leader-follower formation control of multiple non-holonomic mobile robots incorporating a receding-horizon scheme. *Int J Robot Res*. 2010;29(6):727-747.
21. Yu P, Ding L, Liu ZW, Guan ZH. Leader–follower flocking based on distributed event-triggered hybrid control. *Int J Robust Nonlinear Control*. 2016;26(1):143-153.
22. Li Z, Ren W, Liu X, Fu M. Distributed containment control of multi-agent systems with general linear dynamics in the presence of multiple leaders. *Int J Robust Nonlinear Control*. 2013;23(5):534-547.
23. Li Z, Duan Z, Ren W, Feng G. Containment control of linear multi-agent systems with multiple leaders of bounded inputs using distributed continuous controllers. *Int J Robust Nonlinear Control*. 2015;25(13):2101-2121.
24. Tanner HG. On the controllability of nearest neighbor interconnections. Paper presented at: Proceedings of the 43rd IEEE Conference on Decision and Control; vol 3, 2004:2467-2472.
25. Yu W, Chen G, Cao M. Distributed leader–follower flocking control for multi-agent dynamical systems with time-varying velocities. *Syst Control Lett*. 2010;59(9):543-552.
26. Khalili M, Zhang X, Cao Y, Polycarpou MM, Parisini T. Distributed adaptive fault-tolerant leader-following formation control of nonlinear uncertain second-order multi-agent systems. *Int J Robust Nonlinear Control*. 2018;28(15):4287-4308.
27. Xie D, Yuan D, Lu J, Zhang Y. Consensus control of second-order leader–follower multi-agent systems with event-triggered strategy. *Trans Inst Measur Control*. 2013;35(4):426-436.
28. Chen X, Yan P, Serrani A. On input-to-state stability-based design for leader/follower formation control with measurement delays. *Int J Robust Nonlinear Control*. 2013;23(13):1433-1455.
29. Kownacki C, Ambroziak L. Flexible structure control scheme of a UAVs formation to improve the formation stability during maneuvers. *Acta Mechanica et Automatica*. 2017;11(3):178-185.
30. Ren W, Beard RW. Trajectory tracking for unmanned air vehicles with velocity and heading rate constraints. *IEEE Trans Control Syst Tech*. 2004;12(5):706-716.
31. Panteley E, Lefeber E, Loria A, Nijmeijer H. Exponential tracking control of a mobile car using a cascaded approach. *IFAC Proc Vol*. 1998;31(27):201-206.
32. Jiang ZP, Nijmeijer H. Tracking control of mobile robots: a case study in backstepping. *Automatica*. 1997;33(7):1393-1399.
33. Loria A, Dasdemir J, Jarquin NA. Leader–follower formation and tracking control of mobile robots along straight paths. *IEEE Trans Control Syst Tech*. 2015;24(2):727-732.
34. Defoort M, Floquet T, Kokosy A, Perruquetti W. Sliding-mode formation control for cooperative autonomous mobile robots. *IEEE Trans Ind Electron*. 2008;55(11):3944-3953.
35. Liu T, Jiang ZP. Distributed formation control of nonholonomic mobile robots without global position measurements. *Automatica*. 2013;49(2):592-600.
36. Yu X, Liu L. Distributed formation control of nonholonomic vehicles subject to velocity constraints. *IEEE Trans Ind Electron*. 2015;63(2):1289-1298.
37. Khalil HK. *Nonlinear Systems*. Upper Saddle River, NJ: Prentice-Hall; 2002.
38. Tanner HG, Pappas GJ, Kumar V. Leader-to-formation stability. *IEEE Trans Robot Automat*. 2004;20(3):443-455.

SUPPORTING INFORMATION

Additional supporting information may be found online in the Supporting Information section at the end of this article.

How to cite this article: Wang X, Yu Y, Li Z. Distributed sliding mode control for leader-follower formation flight of fixed-wing unmanned aerial vehicles subject to velocity constraints. *Int J Robust Nonlinear Control*. 2020;1–16. https://doi.org/10.1002/rnc.5030